

Communication pubs.acs.org/JACS

Fluorescence-Detected Circular Dichroism of a Chiral Molecular Monolayer with Dielectric Metasurfaces

Michelle L. Solomon,* John M. Abendroth, Lisa V. Poulikakos, Jack Hu, and Jennifer A. Dionne*



Cite This: J. Am. Chem. Soc. 2020, 142, 18304-18309



ACCESS I

Metrics & More

Article Recommendations

Supporting Information

ABSTRACT: Strong enhancement of molecular circular dichroism (CD) has the potential to enable efficient asymmetric photolysis, a method of chiral separation that has conventionally been impeded by insufficient yield and low enantiomeric excess. Here, we study experimentally how predicted enhancements in optical chirality density near resonant silicon nanodisks boost CD. We use fluorescence-detected circular dichroism (FDCD) spectroscopy to measure indirectly the differential absorption of circularly polarized light by a monolayer of optically active molecules functionalized to silicon nanodisk arrays. Importantly, the molecules and nanodisk antennas have spectrally coincident resonances, and our fluorescence technique allows us to deconvolute absorption in the nanodisks from the molecules. We find that enhanced FDCD signals depend on nanophotonic resonances, in good agreement with simulated differential absorption and optical chirality density, while no signal is detected from molecules adsorbed on featureless silicon surfaces. These results verify the potential of nanophotonic platforms to be used for asymmetric photolysis with lower energy requirements.

hirality, or handedness, is a fundamental property of all ✓ living organisms, from biological building blocks such as DNA and amino acids to macroscopic structures. Chirality also features prominently in many synthetic molecules, with over 50% of pharmaceuticals and 40% of agrochemicals existing as enantiopure forms or racemic mixtures. 1,2 These enantiomers can have distinct efficacy in biological systems, making the ability to distinguish mirror-image molecules with high sensitivity and maximize enantiomeric excess (ee) in asymmetric synthesis crucial tasks. Circular dichroism (CD), defined as the selective absorption of circularly polarized light (CPL), is commonly used to differentiate enantiomers via CD spectroscopy, though it typically requires relatively high sample concentrations or long optical path lengths.^{3,4} This differential absorption between left- and right-CPL, $A^{L} - A^{R}$ (ΔA), has also inspired efforts to use CPL as a reagent in enantioselective synthesis or for photolysis as early as 1929.^{5,6} However, due to the low differential absorption cross section of molecules, the yield and ee achieved by decomposition of optical isomers with light alone falls below industrially relevant state-of-the-art techniques to maximize enantiopurity.

A variety of methods have sought to improve the sensitivity of chiral differentiation in CD spectroscopy. For example, nonlinear spectroscopies utilizing second harmonic generation that are sensitive to surfaces and interfaces 10-12 and singlemolecule spectroscopy have enabled enantiomeric detection at the monolayer to few- to single-molecule regime. 13,14 To expand upon these spectroscopic techniques, superchiral electromagnetic fields arising from the interference of chiral plane waves have been shown to increase dissymmetry in chiral excitation, but the position of the superchiral fields within the resulting standing wave nodes limits utility. 15,16 Recently, nanophotonic architectures have received considerable attention due to their potential to manipulate chiral evanescent near fields while maintaining high field strength. 17-26 These near fields have been predicted to enhance the enantioselective rates of molecular absorption and can be achieved using plasmonic^{27–34} and high-refractive-index nanostructures.^{35–41} In experiments, many of these approaches enable highly effective enantiomeric sensors but often exhibit negligible spectral overlap between chiral molecular absorption and nanoantenna resonances, which is necessary to achieve enantioselective photolysis with high yield and ee. 36,37,42 Therefore, rather than enhancing differential absorption rates by the molecules themselves, resulting CD signals in the visible and near-IR are mainly due to intrinsic (extrinsic) chirality of 3D (2D) nanostructures, or induced CD in lossy platforms.⁴³ Furthermore, these techniques struggle to distinguish molecular absorption from total absorption, making it difficult to unveil and optimize the near-field mechanism behind chiraloptical enhancements in molecules. 44,45

Here, we demonstrate enhanced enantioselective absorption in chiral molecular monolayers using nanostructures with optical resonances spectrally matched to the molecular CD. Sub-wavelength, periodic arrays of silicon disks (hereafter, "metasurfaces") are functionalized with self-assembled monolayers of fluorescently labeled oligonucleotide strands with visible-frequency CD (see Figure 1a), attributed to dye binding within the helical DNA environment. We use fluorescencedetected circular dichroism (FDCD) to perform a background-

Received: July 9, 2020 Published: October 13, 2020





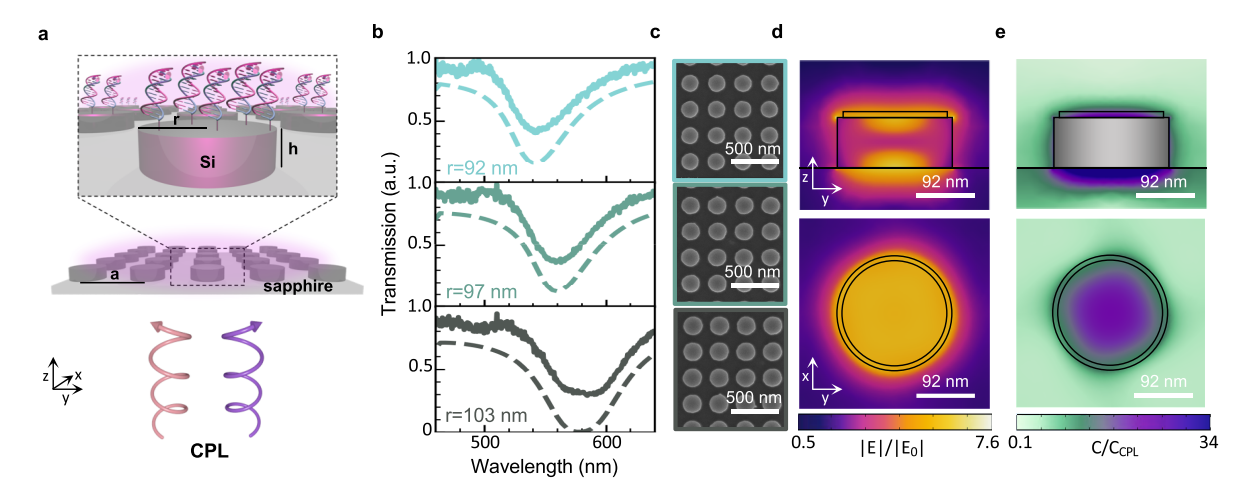


Figure 1. (a) Schematic: dye/DNA functionalized to metasurface. (b) Array transmission: radius, r = 92-103 nm, height, h = 80 nm, pitch, a = 300 nm. (c) Array SEMs. (d) Electric field enhancement on resonance, $\lambda = 570$ nm. (e) Maximized C enhancement, $\lambda = 565$ nm. (d, e) r = 92 nm metasurface; top through disk center; bottom 5 nm above disk/layer interface. Simulated chiral layer radius is $r_l = 82$ nm, avoiding mesh artifacts at disk edge, with layer height, $h_l = 10$ nm.

free measurement, as the dye fluorescence is distinguishable from that in the metasurface or substrate. While negligible FDCD is observed on unpatterned films, we observe strong, red-shifting FDCD on disks with increasing radius, in agreement with calculations. We show that our method can distinguish conformation in molecular monolayers, which we validate with *in situ* measurements of FDCD sign reversal during DNA dehybridization. Our results exhibit enhancement of intrinsic molecular CD, en route to enantioselective photolysis.

Metasurfaces were engineered to have concurrent electric and magnetic dipolar Mie resonances coinciding with the molecular monolayer absorption, a condition known as the first Kerker condition, at which optical chirality density was found to be highly enhanced in our previous work.³⁷ These overlapping modes enhance optical chirality density due to strong electric and magnetic near fields that maintain the phase properties of incident CPL, and disk nanoantennas enable facile tuning of such resonances (see Supporting Information (SI) and Figure S1 for further detail). 37,38,45-51 Nanodisk arrays were fabricated in single-crystalline silicon layers grown on sapphire substrates. The fabricated arrays are 100 μ m \times 100 μ m, with nominal disk height h=80 nm, disk radii r=90-105nm, and pitch a = 300 nm. Figure 1b includes experimental transmission spectra of three examples of bare silicon metasurfaces with nominal disk radii of r = 92, 97, and 103 nm, with representative SEMs in Figure 1c. We simulate these metasurfaces with a layer of chiral medium on top, where layer height $h_1 = 10$ nm, and layer radius $r_1 = r - 10$ nm (see SI), finding that the simulated transmission (dotted line, Figure 1b) is in good agreement with experiments. Dips in the transmission spectra correspond to concurrent electric and magnetic Mie resonances; the simulated electric field plots of Figure 1d are indicative of these overlapping resonances and show strong electric fields extending into the chiral layer.³⁷ Near these resonances, and just blue-shifted ($\lambda = 565$ nm vs λ = 570 nm), optical chirality density in the chiral layer reaches a maximum enhancement (Figure 1e). Here, we define the optical chirality density as $C = -\frac{\omega}{2} \text{Im}(\mathbf{D}^* \cdot \mathbf{B})$ and the enhancement factor as C/C_{CPL} , where $C_{CPL} = \frac{\epsilon_0 \omega}{2\epsilon} E_0^2$, the

optical chirality density of CPL alone. 16,18,52 The small shift between peak $C/C_{\rm CPL}$ and resonance center wavelength occurs due to the balance between the relative phases and intensities of the electric and magnetic fields. 36

The fluorophore, ATTO 590, was covalently attached to the 5'-end of a 25 base pair DNA sequence with a thiol modification on the 3'-end (Figure 2a, see SI for details). The complex absorbs strongly from 500 to 650 nm, with a peak in excitation at 600 nm and an emission maximum at 615 nm that depends on the excitation wavelength (Figure 2b,c). When hybridized with its fully complementary strand, the dye-

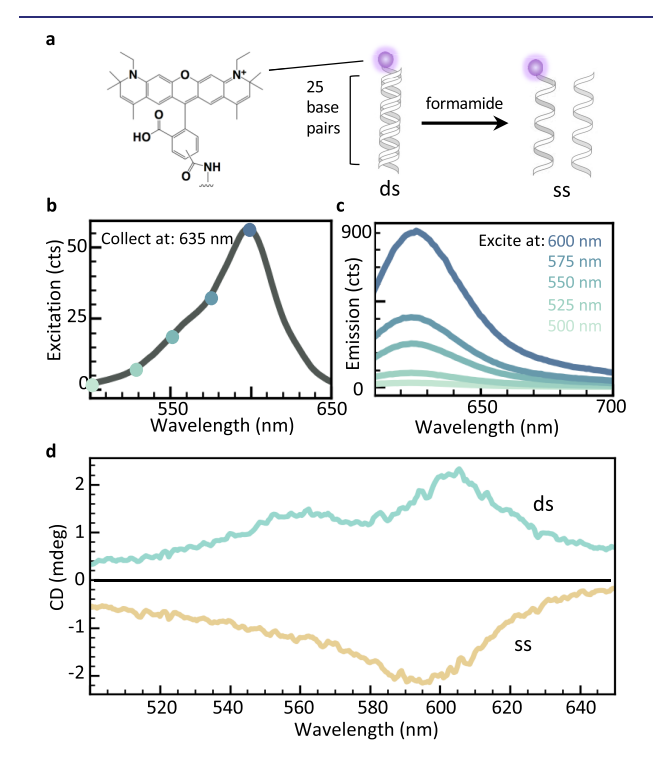


Figure 2. (a) Structure of Atto590 dye functionalized to the 5'-end of DNA and dehybridization scheme. (b) Excitation spectrum of dyedsDNA in PBS. (c) Emission spectra of dye-dsDNA in PBS. (d) CD of dye-dsDNA and dye-ssDNA in PBS, 30 μ M.

dsDNA complex exhibits a positive CD signal in its visible absorption band. S1-56 Interestingly, the sign of the CD signal is reversed when the DNA molecules are denatured, as the dye molecules experience the different local environment of the single strand's secondary structure (Figures 2d and S2). This enantiomer-reversal-like behavior is particularly useful to probe changes in the sign of the CD signal on the same substrates without varying surface density.

The metasurfaces were functionalized with self-assembled monolayers of the dye-DNA complexes with widely used silane chemistry (Figure 3a). ^{58,59} Terminal amine groups on vapor-

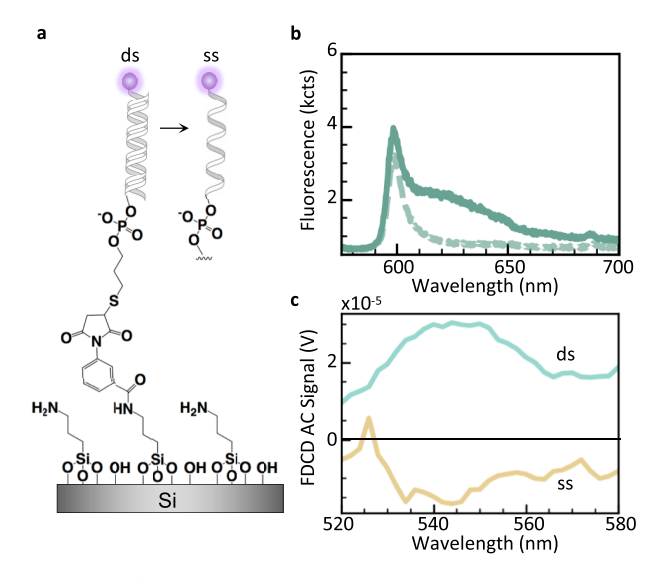


Figure 3. (a) Functionalization scheme and dehybridization on substrate. (b) Fluorescence of dye-functionalized 92 nm-radius array (solid) vs dye-less (dotted). (c) FDCD sign reversal from dye-dsDNA to dye-ssDNA.

deposited films of (3-aminopropyl)trimethoxysilane were cross-linked to pre-hybridized thiol-modified DNA strands using m-maleimidobenzoyl-N-hydroxysuccinimide ester (see SI). Monolayers of DNA prepared by silanization on Si/SiO₂ typically feature surface densities of $\sim 10^{12}$ molecules/cm², which represents an approximate upper bound to the limit of detection of our technique. To validate surface functionalization, metasurface fluorescence spectra were collected both before and after DNA assembly. Strong fluorescence near the long-pass edge at 600 nm can be attributed to background fluorescence from the sapphire substrate. However, a significant increase in emission intensity from 610 to 650 nm following functionalization confirms that fluorescence from the monolayer is distinguishable from that of the substrate (Figure 3b).

To detect the CD of the monolayers indirectly using fluorescence, we built a table-top polarization-sensitive spectrometer that performs a lock-in measurement to collect excitation spectra (see SI). For this measurement, we used a 635 nm bandpass filter that transmits the fluorescence of the dye alone. First, we studied the FDCD signal dependence on the hybridization state of the DNA monolayers which, from solution/ensemble-CD measurements, reverses sign between double- and single-stranded forms. Monolayer-functionalized metasurfaces were mounted within a cuvette of 1× phosphate-buffered saline (PBS) to maintain the helical tertiary structure of dsDNA when tethered to surfaces during measurements

(Figure S3). Using metasurfaces functionalized with dyedsDNA complexes, positive FDCD signals were measured in the range of 520 to 580 nm for each of the different radii (Figures 3c and S4). Then, PBS was removed and replaced with formamide to lower the DNA melting temperature below room temperature. Upon denaturing, the FDCD signal reversed sign or was destroyed completely (Figures 3c and S4). Importantly, because the dye-functionalized ssDNA remains tethered to the surfaces, the change in FDCD signal can be attributed to partial or complete dehybridization of adsorbed DNA rather than removal of fluorescent probes from the surfaces.

We repeated the double-stranded DNA measurements on the three metasurfaces characterized in Figure 1 to study the spectral influence of the metasurface resonance on the FDCD signal. These results (Figure 4a) show a red-shifting FDCD

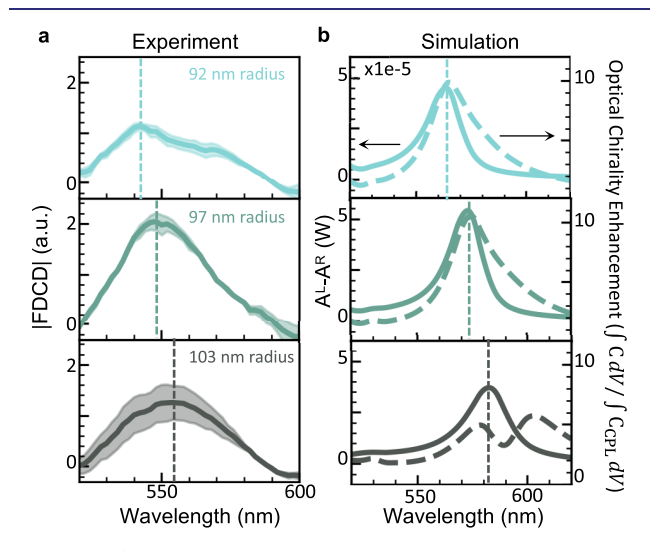


Figure 4. (a) Normalized FDCD signal from dye-dsDNA on r=92-103 nm arrays (details in SI). Vertical lines mark spectra maxima, illustrating red-shift; shaded region represents standard error. (b) Simulated ΔA from 10 nm chiral layer on disk surface (left axis, solid) against integrated $C/C_{\rm CPL}$ (right axis, dotted). Vertical lines mark ΔA maxima.

signal with increasing disk size. Consistent with C/C_{CPL} in Figure 1, the peak is blue-shifted from the resonance center wavelength. In contrast, upon repeating the measurement on an identically sized square of unpatterned silicon on the same sapphire substrate, no significant FDCD signal is observed (Figure S5), illustrating that the detected signal can primarily be attributed to the electromagnetic near-field enhancements. To confirm that the measured FDCD signal arises primarily from molecular CD, we performed full-field simulations, calculating ΔA and C/C_{CPL} within a 10-nm-thick chiral layer above the silicon disks. To account for coupling effects between induced electric and magnetic dipoles in the chiral medium, these simulations used a wavelength-independent Pasteur parameter with strength typical of an on-resonant chiral molecule (see SI). 32,34,45 Figure 4b shows these results, indicating that the peak in molecular ΔA occurs just blueshifted from the dip in transmission and red shifts with increasing disk size, corresponding well with experiments. Further, the observed line shape and spectral position of the simulated ΔA are in good agreement with those of the optical chirality enhancement in the molecular layer, seen in the solid

and dotted lines of Figure 4b, respectively. We note that the optical chirality calculated in the chiral layer on the 103 nm metasurface exhibits two peaks, in contrast to the single peak in ΔA , likely due to higher enhancements in electric field associated with the blue-shifted mode as the resonances separate. Importantly, ΔA within the silicon nanodisks in simulation (Figure S6) is given by a bisignate line shape not seen in our measurement. This result further indicates that the measured FDCD signal arises primarily from enhanced molecular CD due to high optical chirality density in the near field, as opposed to induced CD in the disks themselves.⁴⁴ We attribute the non-negligible (~20 nm) red shift between simulation and experiment to a combination of an oxide layer on the silicon surface, tapering of disk side-walls, and wavelength-dependent chiral medium properties which were not captured in our model.

In summary, we demonstrate enhancement of intrinsic molecular CD in a monolayer via overlap of molecular CD with nanophotonic resonances using FDCD. We study the CD of ATTO 590-functionalized DNA strands, with a solutionphase CD signal from 500 to 650 nm. Interestingly, the sign of this CD signal is dependent on DNA conformation, with dyedsDNA exhibiting a positive signal and dye-ssDNA exhibiting a negative signal. The complexes are functionalized to silicon metasurfaces fabricated with optical resonances in the CD band of interest and characterized using a table-top FDCD spectrometer. We exploit the enantiomer-reversal-like behavior of the different conformations to probe surface chirality by dehybridizing the dsDNA, observing a sign reversal when metasurfaces are present but negligible signal in their absence. Finally, we show that the FDCD signal red shifts with increasing disk size, and thus that the metasurface's resonant features are central to molecular CD enhancement. Full-field simulations confirm that both differential absorption and optical chirality density are enhanced within the chiral medium near the disk resonances. This indicates that the experimental FDCD enhancement is due to enhanced optical chirality density, as predicted in prior works, thus providing important insights toward efficient enantioselective photolysis.

ASSOCIATED CONTENT

Supporting Information

The Supporting Information is available free of charge at https://pubs.acs.org/doi/10.1021/jacs.0c07140.

Materials and methods, summary of findings of dye-DNA functionalized to unpatterned silicon, simulation details, and raw data and data analysis procedure, as well as additional data (PDF)

AUTHOR INFORMATION

Corresponding Authors

Michelle L. Solomon — Materials Science and Engineering, Stanford University, Stanford, California 94305, United States; orcid.org/0000-0002-8123-7557; Email: msolomo8@stanford.edu

Jennifer A. Dionne — Materials Science and Engineering, Stanford University, Stanford, California 94305, United States; orcid.org/0000-0001-5287-4357; Email: jdionne@stanford.edu

Authors

John M. Abendroth — Materials Science and Engineering, Stanford University, Stanford, California 94305, United States Lisa V. Poulikakos — Materials Science and Engineering, Stanford University, Stanford, California 94305, United States; Mechanical and Aerospace Engineering, University of California San Diego, La Jolla, California 92093, United States; orcid.org/0000-0002-1118-789X

Jack Hu — Materials Science and Engineering, Stanford University, Stanford, California 94305, United States; orcid.org/0000-0001-7515-0386

Complete contact information is available at: https://pubs.acs.org/10.1021/jacs.0c07140

Notes

The authors declare no competing financial interest.

ACKNOWLEDGMENTS

The authors thank Dr. Mark Lawrence, Dr. Aitzol Garcia-Etxarri, Dr. Michal Vadai, Dr. Claire McClellan, and David Barton for insightful discussions. The authors gratefully acknowledge the Gordon and Betty Moore Foundation for funding through a Moore Inventors Fellowship under grant number 6881, and the National Science Foundation under grant number 1905209. M.L.S. acknowledges a National Defense Science and Engineering graduate fellowship. L.V.P. acknowledges support from a Swiss National Science Foundation Early Postdoc Mobility fellowship under project number P2EZP2 181595. Work was performed in part in the nano@Stanford laboratories (Stanford Nano Shared Facilities and the Stanford Nanofabrication Facility), which are supported by the National Science Foundation as part of the National Nanotechnology Coordinated Infrastructure under award ECCS-1542152.

REFERENCES

- (1) Nguyen, L. A.; He, H.; Pham-Huy, C. Chiral drugs: an overview. *Int. J. Biomed. Sci.: IJBS* **2006**, *2*, 85–100.
- (2) Jeschke, P. Current status of chirality in agrochemicals. *Pest Manage. Sci.* **2018**, 74, 2389–2404.
- (3) Kelly, S. M.; Jess, T. J.; Price, N. C. How to study proteins by circular dichroism. *Biochim. Biophys. Acta, Proteins Proteomics* **2005**, 1751, 119–139.
- (4) Zhao, Y.; Askarpour, A. N.; Sun, L.; Shi, J.; Li, X.; Alù, A. Chirality detection of enantiomers using twisted optical metamaterials. *Nat. Commun.* **2017**, *8*, 14180.
- (5) Kuhn, W.; Braun, E. Photochemische erzeugung optisch aktiver stoffe. *Naturwissenschaften* 1929, 17, 227–228.
- (6) Feringa, B.; Wynberg, H. Biomimetic asymmetric oxidative coupling of phenols. *Bioorg. Chem.* **1978**, *7*, 397–408.
- (7) Inoue, Y. Asymmetric photochemical reactions in solution. *Chem. Rev.* **1992**, 92, 741–770.
- (8) Flores, J. J.; Bonner, W. A.; Massey, G. A. Asymmetric photolysis of (RS)-leucine with circularly polarized ultraviolet light. *J. Am. Chem. Soc.* 1977, 99, 3622–3625.
- (9) Balavoine, G.; Moradpour, A.; Kagan, H. Preparation of chiral compounds with high optical purity by irradiation with circularly polarized light, a model reaction for the prebiotic generation of optical activity. *J. Am. Chem. Soc.* **1974**, *96*, 5152–5158.
- (10) Lin, L.; Wang, T.; Lu, Z.; Liu, M.; Guo, Y. In situ measurement of the supramolecular chirality in the langmuir monolayers of achiral porphyrins at the air/aqueous interface by second harmonic generation linear dichroism. *J. Phys. Chem. C* **2014**, *118*, 6726–6733.
- (11) Burke, B. J.; Moad, A. J.; Polizzi, M. A.; Simpson, G. J. Experimental confirmation of the importance of orientation in the

- anomalous chiral sensitivity of second harmonic generation. *J. Am. Chem. Soc.* **2003**, *125*, 9111–9115.
- (12) Petralli-Mallow, T.; Wong, T.; Byers, J.; Yee, H.; Hicks, J. Circular dichroism spectroscopy at interfaces: a surface second harmonic generation study. *J. Phys. Chem.* **1993**, *97*, 1383–1388.
- (13) Hassey-Paradise, R.; Cyphersmith, A.; Tilley, A. M.; Mortsolf, T.; Basak, D.; Venkataraman, D.; Barnes, M. D. Dissymmetries in fluorescence excitation and emission from single chiral molecules. *Chirality* **2009**, *21*, E265–E276.
- (14) Cyphersmith, A.; Surampudi, S.; Casey, M. J.; Jankowski, K.; Venkataraman, D.; Barnes, M. D. Chiroptical dissymmetries in fluorescence excitation from single molecules of (M-2) helicene dimers. *J. Phys. Chem. A* **2012**, *116*, 5349–5352.
- (15) Tang, Y.; Cohen, A. E. Enhanced enantioselectivity in excitation of chiral molecules by superchiral light. *Science* **2011**, 332, 333–336.
- (16) Tang, Y.; Cohen, A. E. Optical chirality and its interaction with matter. *Phys. Rev. Lett.* **2010**, *104*, 163901.
- (17) Gansel, J. K.; Thiel, M.; Rill, M. S.; Decker, M.; Bade, K.; Saile, V.; von Freymann, G.; Linden, S.; Wegener, M. Gold helix photonic metamaterial as broadband circular polarizer. *Science* **2009**, 325, 1513–1515.
- (18) Poulikakos, L. V.; Thureja, P.; Stollmann, A.; De Leo, E.; Norris, D. J. Chiral Light Design and Detection Inspired by Optical Antenna Theory. *Nano Lett.* **2018**, *18*, 4633–4640.
- (19) Esposito, M.; Tasco, V.; Cuscuná, M.; Todisco, F.; Benedetti, A.; Tarantini, I.; de Giorgi, M.; Sanvitto, D.; Passaseo, A. Nanoscale 3D chiral plasmonic helices with circular dichroism at visible frequencies. *ACS Photonics* **2015**, *2*, 105–114.
- (20) Ferry, V. E.; Hentschel, M.; Alivisatos, A. P. Circular dichroism in off-resonantly couple plasmonic nanosystems. *Nano Lett.* **2015**, *15*, 8336–8341.
- (21) Duan, X.; Yue, S.; Liu, N. Understanding complex chiral plasmonics. *Nanoscale* **2015**, *7*, 17237–17243.
- (22) Yao, K.; Liu, Y. Enhancing circular dichroism by chiral hotspots in silicon nanocube dimers. *Nanoscale* **2018**, *10*, 8779–8786.
- (23) Kuzyk, A.; Schreiber, R.; Fan, Z.; Pardatscher, G.; Roller, E.-M.; Högele, A.; Simmel, F. C.; Govorov, A. O.; Liedl, T. DNA-based self-assembly of chiral plasmonic nanostructures with tailored optical response. *Nature* **2012**, *483*, 311–314.
- (24) Govorov, A. O.; Fan, Z.; Hernandez, P.; Slocik, J. M.; Naik, R. R. Theory of circular dichroism of nanomaterials comprising chiral molecules and nanocrystals: plasmon enhancement, dipole interactions, and dielectric effects. *Nano Lett.* **2010**, *10*, 1374–1382.
- (25) Wang, L.-Y.; Smith, K. W.; Dominguez-Medina, S.; Moody, N.; Olson, J. M.; Zhang, H.; Chang, W.-S.; Kotov, N.; Link, S. Circular differential scattering of single chiral self-assembled gold nanorod dimers. *ACS Photonics* **2015**, *2*, 1602–1610.
- (26) Zhao, Y.; Belkin, M. A.; Alù, A. Twisted optical metamaterials for planarized ultrathin broadband circular polarizers. *Nat. Commun.* **2012**, *3*, 870.
- (27) Schäferling, M.; Yin, X.; Engheta, N.; Giessen, H. Helical plasmonic nanostructures as prototypical chiral near-field sources. *ACS Photonics* **2014**, *1*, 530–537.
- (28) Schäferling, M.; Dregely, D.; Hentschel, M.; Giessen, H. Tailoring enhanced optical chirality: Design principles for chiral plasmonic nanostructures. *Phys. Rev. X* **2012**, *2*, 031010.
- (29) Hendry, E.; Carpy, T.; Johnston, J.; Popland, M.; Mikhaylovskiy, R.; Lapthorn, A.; Kelly, S.; Barron, L.; Gadegaard, N.; Kadodwala, M. Ultrasensitive detection and characterization of biomolecules using superchiral fields. *Nat. Nanotechnol.* **2010**, *5*, 783–787
- (30) Hendry, E.; Mikhaylovskiy, R.; Barron, L.; Kadodwala, M.; Davis, T. Chiral electromagnetic fields generated by arrays of nanoslits. *Nano Lett.* **2012**, *12*, 3640–3644.
- (31) Kneer, L. M.; Roller, E.-M.; Besteiro, L. V.; Schreiber, R.; Govorov, A. O.; Liedl, T. Circular dichroism of chiral molecules in DNA-assembled plasmonic hotspots. *ACS Nano* **2018**, *12*, 9110–9115

- (32) García-Guirado, J.; Svedendahl, M.; Puigdollers, J.; Quidant, R. Enantiomer-selective molecular sensing using racemic nanoplasmonic arrays. *Nano Lett.* **2018**, *18*, 6279–6285.
- (33) Tullius, R.; Karimullah, A. S.; Rodier, M.; Fitzpatrick, B.; Gadegaard, N.; Barron, L. D.; Rotello, V. M.; Cooke, G.; Lapthorn, A.; Kadodwala, M. Superchiral" spectroscopy: detection of protein higher order hierarchical structure with chiral plasmonic nanostructures. *J. Am. Chem. Soc.* **2015**, *137*, 8380–8383.
- (34) Nesterov, M. L.; Yin, X.; Schäferling, M.; Giessen, H.; Weiss, T. The role of plasmon-generated near fields for enhanced circular dichroism spectroscopy. *ACS Photonics* **2016**, *3*, 578–583.
- (35) Garcia-Etxarri, A.; Dionne, J. A. Surface-enhanced circular dichroism spectroscopy mediated by nonchiral nanoantennas. *Phys. Rev. B: Condens. Matter Mater. Phys.* **2013**, 87, 235409.
- (36) Ho, C.-S.; Garcia-Etxarri, A.; Zhao, Y.; Dionne, J. Enhancing enantioselective absorption using dielectric nanospheres. *ACS Photonics* **2017**, *4*, 197–203.
- (37) Solomon, M. L.; Hu, J.; Lawrence, M.; García-Etxarri, A.; Dionne, J. A. Enantiospecific optical enhancement of chiral sensing and separation with dielectric metasurfaces. ACS Photonics 2019, 6, 43–49.
- (38) Hu, J.; Lawrence, M.; Dionne, J. A. High Quality Factor Dielectric Metasurfaces for Ultraviolet Circular Dichroism Spectroscopy. *ACS Photonics* **2020**, *7*, 36–42.
- (39) Mohammadi, E.; Tsakmakidis, K. L.; Askarpour, A. N.; Dehkhoda, P.; Tavakoli, A.; Altug, H. Nanophotonic platforms for enhanced chiral sensing. *ACS Photonics* **2018**, *5*, 2669–2675.
- (40) Ben-Moshe, A.; Maoz, B. M.; Govorov, A. O.; Markovich, G. Chirality and chiroptical effects in inorganic nanocrystal systems with plasmon and exciton resonances. *Chem. Soc. Rev.* **2013**, *42*, 7028–7041.
- (41) Zhang, W.; Wu, T.; Wang, R.; Zhang, X. Amplification of the molecular chiroptical effect by low-loss dielectric nanoantennas. *Nanoscale* **2017**, *9*, 5701–5707.
- (42) Balavoine, G.; Moradpour, A.; Kagan, H. Preparation of Chiral Compounds with High Optical Purity by Irradiation with Circularly Polarized Light, a Model Reaction for the Prebiotic Generation of Optical Activity. *J. Am. Chem. Soc.* **1974**, *96*, 5152–5158.
- (43) Lee, S.; Yoo, S.; Park, Q.-H. Microscopic origin of surface-enhanced circular dichroism. *ACS Photonics* **2017**, *4*, 2047–2052.
- (44) Garcia-Guirado, J.; Svedendahl, M.; Puigdollers, J.; Quidant, R. Enhanced chiral sensing with dielectric nano-resonators. *Nano Lett.* **2020**, *20*, 585–591.
- (45) Mohammadi, E.; Tavakoli, A.; Dehkhoda, P.; Jahani, Y.; Tsakmakidis, K. L.; Tittl, A.; Altug, H. Accessible superchiral near-fields driven by tailored electric and magnetic resonances in all-dielectric nanostructures. *ACS Photonics* **2019**, *6*, 1939–1946.
- (46) Graf, F.; Feis, J.; Garcia-Santiago, X.; Wegener, M.; Rockstuhl, C.; Fernandez-Corbaton, I. Achiral, helicity preserving, and resonant structures for enhanced sensing of chiral molecules. *ACS Photonics* **2019**, *6*, 482–491.
- (47) Staude, I.; Miroshnichenko, A. E.; Decker, M.; Fofang, N. T.; Liu, S.; Gonzales, E.; Dominguez, J.; Luk, T. S.; Neshev, D. N.; Brener, I.; Kivshar, Y. Tailoring directional scattering through magnetic and electrical resonances in subwavelength silicon nanodisks. *ACS Nano* **2013**, *7*, 7824–7832.
- (48) Siday, T.; Vabishchevich, P. P.; Hale, L.; Harris, C. T.; Luk, T. S.; Reno, J. L.; Brener, I.; Mitrofanov, O. Terahertz detection with perfectly-absorbing photoconductive metasurface. *Nano Lett.* **2019**, 19, 2888–2896.
- (49) Yang, C.-Y.; Yang, J.-H.; Yang, Z.-Y.; Zhou, Z.-X.; Sun, M.-G.; Babicheva, V. E.; Chen, K.-P. Nonradiating silicon nanoantenna metasurfaces as narrowband absorbers. *ACS Photonics* **2018**, *5*, 2596—2601.
- (50) Decker, M.; Staude, I.; Falkner, M.; Dominguez, J.; Neshev, D. N.; Brener, I.; Pertsch, T.; Kivshar, Y. S. High-efficiency dielectric Huygens' surfaces. *Adv. Opt. Mater.* **2015**, *3*, 813–820.

- (51) Decker, M.; Staude, I. Resonant dielectric nanostructures: a low-loss platform for functional nanophotonics. *J. Opt.* **2016**, *18*, 103001.
- (52) Barron, L. D. Molecular Light Scattering and Optical Activity; Cambridge University Press, 2009.
- (53) Kringle, L.; Sawaya, N. P.; Widom, J.; Adams, C.; Raymer, M. G.; Aspuru-Guzik, A.; Marcus, A. H. Temperature-dependent conformations of exciton-coupled Cy3 dimers in double-stranded DNA. J. Chem. Phys. 2018, 148, 085101.
- (54) Nordén, B.; Tjerneld, F. Structure of methylene blue–DNA complexes studied by linear and circular dichroism spectroscopy. *Biopolymers* **1982**, *21*, 1713–1734.
- (55) Neelakandan, P. P.; Zeidan, T. A.; McCullagh, M.; Schatz, G. C.; Vura-Weis, J.; Kim, C. H.; Wasielewski, M. R.; Lewis, F. D. Ground and excited state electronic spectra of perylenediimide dimers with flexible and rigid geometries in DNA conjugates. *Chemical Science* 2014, 5, 973–981.
- (56) Tuite, E. M.; Nordén, B. Linear and circular dichroism characterization of thionine binding mode with DNA polynucleotides. *Spectrochim. Acta, Part A* **2018**, *189*, 86–92.
- (57) Stokes, G. Y.; Gibbs-Davis, J. M.; Boman, F. C.; Stepp, B. R.; Condie, A. G.; Nguyen, S. T.; Geiger, F. M. Making "sense" of DNA. *J. Am. Chem. Soc.* **2007**, *129*, 7492–7493.
- (58) Nakatsuka, N.; Yang, K.-A.; Abendroth, J. M.; Cheung, K. M.; Xu, X.; Yang, H.; Zhao, C.; Zhu, B.; Rim, Y. S.; Yang, Y.; Weiss, P. S.; Stojanović, M. N.; Andrews, A. M. Aptamer—field-effect transistors overcome Debye length limitations for small-molecule sensing. *Science* **2018**, 362, 319—324.
- (59) Cheung, K. M.; Abendroth, J. M.; Nakatsuka, N.; Zhu, B.; Yang, Y.; Andrews, A. M.; Weiss, P. S. Detecting DNA and RNA and Differentiating Single-Nucleotide Variations via Field-Effect Transistors. *Nano Lett.* **2020**, 20, 5982–5990.
- (60) Strother, T.; Cai, W.; Zhao, X.; Hamers, R. J.; Smith, L. M. Synthesis and characterization of DNA-modified silicon (111) surfaces. J. Am. Chem. Soc. 2000, 122, 1205–1209.
- (61) Pirrung, M. C. How to make a DNA chip. Angew. Chem., Int. Ed. 2002, 41, 1276–1289.